Journal of Biomolecular NMR (2006) 36: 13–26
DOI 10.1007/s10858-006-9056-3

Article

Towards unambiguous assignment of methyl-containing residues by double and triple sensitivity-enhanced HCCmHm-TOCSY experiments

Peter Würtz, Maarit Hellman, Helena Tossavainen & Perttu Permi*
Program in Structural Biology and Biophysics, Institute of Biotechnology/NMR Laboratory, University of Helsinki, P.O. Box 65, FI-00014, Helsinki, Finland

Received 19 April 2006; Accepted 14 July 2006

Key words: assignment, coactosin, coherence transfer, HCCH-TOCSY, methyl groups, NMR spectroscopy, proteins

Abstract

Chemical shift assignment of methyl-containing residues is essential in protein NMR spectroscopy, as these residues are abundant in protein interiors and provide the vast majority of long-range NOE connectivities for structure determination. These residues also constitute an integral part of hydrophobic cavities, the surroundings for many enzymatic reactions. Here we present a powerful strategy for the assignment of methyl-containing residues in a uniformly $^{13}C/^{15}N$ double labeled protein sample. The approach is based on novel four-dimensional HCCmHm-TOCSY experiments, two of them utilizing gradient selection and sensitivity enhancement in all three indirectly detected dimensions. Regardless of the number of dimensions, the proposed experiments can be executed using only one transient per FID, providing outstanding resolution and sensitivity. A complete assignment of the 51 methyl-containing residues in the 16 kDa *Mus musculus* coactosin was accomplished using a four-dimensional HCCmHm-TOCSY spectrum recorded in 16 hours.

Introduction

Methyl-containing and aromatic residues form the core of a protein, and provide hydrophobic cavities in protein interiors where enzymatic reactions occur. The ligand binding epitope of a protein can be characterized by monitoring methyl group chemical shift changes in interaction studies (Hajduk et al., 2000). In addition, methyl-methyl and methyl-amide NOEs are vital for structure determination (Mueller et al., 2000). Consequently, development of robust methodology for efficient assignment of methyl group chemical shifts is readily justified. Conventional approaches for assigning methyl-containing residues are based on either three-dimensional ^{13}C-^{1}H detected HC(C)H-TOCSY and H(C)CH-COSY experiments (Bax et al., 1990a, b, Fesik et al., 1990; Kay et al., 1990a, b; Montelione et al. 1992) or ^{15}N-$^{1}H^{N}$ detected (H)CC(CO)NH-TOCSY and H(CC)NH-TOCSY /H(CC)(CO)NH-TOCSY experiments (Lyons and Montelione, 1993; Grzesiek et al., 1993, Logan et al., 1993; Gardner et al., 1996; Liu and Wagner, 1999). The former approach provides superior sensitivity whereas merits of latter lie in the excellent resolution of ^{15}N and $^{1}H^{N}$ dimensions and efficient water suppression obtained by sensitivity-enhanced gradient selection. However, no direct H-C connectivities are observed, and typically this information is

*To whom correspondence should be addressed. E-mail: Perttu.Permi@helsinki.fi

gathered e.g. using a HC(C)H-COSY experiment. A four dimensional HCC(CO)NNH-TOCSY experiment (Clowes et al., 1993) has been proposed, which simultaneously provides direct sidechain proton–carbon connectivities and relates these to a backbone amide group. The sensitivity of this experiment is inherently lower than its three dimensional counterparts. The amide proton detected ^{13}C-^{13}C TOCSY type of experiments in general suffer from sensitivity losses related to inefficient ^{13}C-^{13}C TOCSY transfer and long transfer steps from ^{13}C to ^{15}N. The latter can be improved by selective methyl protonation (Gardner et al., 1997a, b; Goto et al., 1999) and simultaneous use of the TROSY approach (Pervushin et al., 1997, Hilty et al., 2002). However, this procedure is not very cost-efficient if the protein expression level is modest or even moderately low. Furthermore, the gain in sensitivity is negatively counterbalanced by the rapid transverse relaxation of the $^{13}C'$ spin at the field strength optimal for the TROSY effect (Permi and Annila, 2004). If a (H)CCNH-TOCSY experiment is used instead, both the intraresidual and sequential coherence transfer pathways are effective, which doubles the number of observable cross peaks. The ^{13}C–^{1}H detected experiments offer an alternative approach with improved sensitivity. Tugarinov and Kay have proposed several ^{13}C–^{13}C COSY based experiments together with new labeling schemes for Leu and Val residues to assign selectively protonated methyl resonances (Tugarinov and Kay, 2003a, b). Methyl TROSY experiment was proposed by the same group for recording ^{1}H–^{13}C correlations in highly deuterated, methyl protonated larger proteins (Tugarinov et al., 2004).

Uhrín and his co-workers suggested an approach based on linking methyl group ^{13}C and ^{1}H chemical shifts with those of $^{13}C^{\alpha}$ and $^{13}C^{\beta}$ (Uhrin et al., 2000; Yang et al., 2004). In these experiments, $^{13}C^{\alpha}$ and $^{13}C^{\beta}$ magnetization is relayed to methyl carbons by a ^{13}C–^{13}C TOCSY transfer. The ^{13}C methyl resonances are subsequently frequency labeled during a relatively long (~28 ms) constant-time period, followed by proton detection. Inspired by this approach, our group recently proposed a gradient selected and double sensitivity-enhanced DE-MQ-(H)CCmHm-TOCSY implementation of this experiment with which we were able to assign 75 out of the 77 methyl groups of a 142-residue protein (Permi et al., 2004). In this paper we propose a new assignment strategy based on single transient 4D spectroscopy. Four new pulse sequences for the assignment of methyl-containing residues are presented, a three-dimensional Gradient selected Double sensitivity Enhanced (GDE) H(C)CmHm-TOCSY scheme to complement the three-dimensional DE-MQ-(H)CCmHm-TOCSY (Permi et al., 2004), and three different implementations of a four-dimensional HCCmHm-TOCSY experiment with Gradient selection and Double or Triple sensitivity Enhancement (GDE-HCCmHm-TOCSY or GTE-HCCmHm-TOCSY). Spectra with good resolution and sensitivity are obtained in short acquisition times using a single transient, efficiently providing unambiguous methyl assignments.

Theory

The three-dimensional GDE-H(C)CmHm-TOCSY experiment is shown in Figure 1a, whereas Figure 1b–d illustrate different implementations of four-dimensional HCCmHm-TOCSY experiments used in this study. These experiments are based on the $HCCH_3$ (Uhrín et al., 2000) double sensitivity enhanced H(C)CH-TOCSY (Sattler et al., 1995a) and DE-MQ-(H)CCmHm (Permi et al., 2004) experiments. In the following we will briefly describe the main course of the proposed experiments and emphasize the differing features providing the improved resolution and sensitivity with respect to the original schemes. The major difference between the four-dimensional implementations stems from gradient selection, i.e. schemes shown in Figure 1b and c utilize gradient selection in all three indirectly detected dimensions whereas in the scheme in Figure 1d sensitivity-enhanced gradient selection is employed in two indirectly detected dimensions. Schemes 1b and 1c are referred here to as GTE-HCCmHm-TOCSY (Gradient selected, Triple sensitivity Enhanced) and scheme 1d to as GDE-HCCmHm-TOCSY (Gradient selected, Double sensitivity Enhanced).

The course of the three-dimensional GDE-H(C)CmHm-TOCSY experiment (Figure 1a) can be described in the following way

$$^{1}H(\mathrm{SCT}-t_1)\xrightarrow{zxy\text{–ICOS–CT}(^{1}J_{\mathrm{HC}})}{}^{13}\mathrm{C}\xrightarrow{\mathrm{C,C\text{–TOCSY}}}{}^{13}\mathrm{C}_m(\mathrm{CT}-t_2)\xrightarrow{yxz\text{–ICOS–CT}(^{1}J_{\mathrm{CmHm}})}{}^{1}\mathrm{H}_m(t_3).$$

The coherence transfer can be described analogously for the three four-dimensional experiments: GTE-HCCmHm-TOCSY (Figure 1b and 1c):

$$^{1}H(\mathrm{SCT}-t_1)\xrightarrow{zxy\text{–ICOS–CT}(^{1}J_{\mathrm{HC}})}{}^{13}\mathrm{C}(t_2)\xrightarrow{\mathrm{C,C\text{–TOCSY}}}{}^{13}\mathrm{C}_m(\mathrm{CT}-t_3)\xrightarrow{yxz\text{–ICOS–CT}(^{1}J_{\mathrm{CmHm}})}{}^{1}\mathrm{H}_m(t_4)$$

and

$$^{1}\mathrm{H}(t_1)\xrightarrow{yxz\text{–ICOS–CT}(^{1}J_{\mathrm{HC}})}{}^{13}C(\mathrm{SCT}-t_2)\xrightarrow{\mathrm{C,C\text{–TOCSY}}}{}^{13}\mathrm{C}_m(\mathrm{CT}-t_3)\xrightarrow{yxz\text{–ICOS–CT}(^{1}J_{\mathrm{CmHm}})}{}^{1}H_m(t_4),$$

and GDE-HCCmHm-TOCSY (Figure 1d):

$$^{1}H(\mathrm{SCT}-t_1)\xrightarrow{^{1}J_{\mathrm{HC}}}{}^{13}C(\mathrm{SCT}-t_2)\xrightarrow{\mathrm{C,C\text{–TOCSY}}}{}^{13}\mathrm{C}_m(\mathrm{CT}-t_3)\xrightarrow{yxz\text{–ICOS–CT}(^{1}J_{\mathrm{CmHm}})}{}^{1}\mathrm{H}_m(t_4)$$

The couplings and coherence transfer schemes which are employed for the magnetization transfer are shown above the arrows, and t_i (i = 1–4) refer to the acquisition time for the corresponding spin either with a semi-constant time (SCT) or a constant-time (CT) implementation. In the following section, we elaborate on a description of the four-dimensional pulse schemes using the GTE-HCCmHm experiment (Figure 1b) as an example. Differences between the three implementations are also discussed. The course of the three-dimensional GDE-H(C)CmHm-TOCSY experiment (Figure 1a) is very similar and consequently only the differing parts are described.

As a first step, frequencies of aliphatic protons are labeled during the t_1 period implemented as a semi-constant time evolution (Grzesiek and Bax, 1993; Logan et al., 1993). Coherence selection and quadrature detection are established using gradient selection. To this end, a selection gradient (G_S1) is inserted into the first $^{1}J_{CH}$ dephasing delay τ_1, i.e. either $\exp(i\omega_H t_1)$ or $\exp(-i\omega_H t_1)$ modulated signal is selected. This is followed by a coherence order selective coherence transfer (COS-CT) to the adjacent aliphatic carbon spins. Hence, both orthogonal x and y components of magnetization are transferred from ^{1}H to ^{13}C using the zxy-ICOS-CT element (Sattler et al., 1995b). The semi-constant time frequency labeling improves the sensitivity as the delay $2\tau_1$ can be used for chemical shift labeling. The transverse relaxation of protons is effectively scaled down by a factor of $\kappa = (t_{1,\max} - 2\tau_1)/t_{1,\max}$ with respect to a real time evolution period, which partially compensates relaxation mediated sensitivity loss due to the additional $2\tau_2$ period required for the COS-CT implementation.

Labeling of ^{13}C frequencies takes place during the second evolution period, t_2, which immediately follows the first COS-CT step. A pair of dephasing gradients (G_{S2}) is employed for the coherence selection in t_2 and to minimize sensitivity losses due to $^{1}J_{CC}$ modulation and transverse relaxation. At this point, the last 90° pulse on ^{13}C prior to the ensuing isotropic TOCSY mixing sequence converts the y component of magnetization to z-magnetization. Obviously, chemical shift labeling

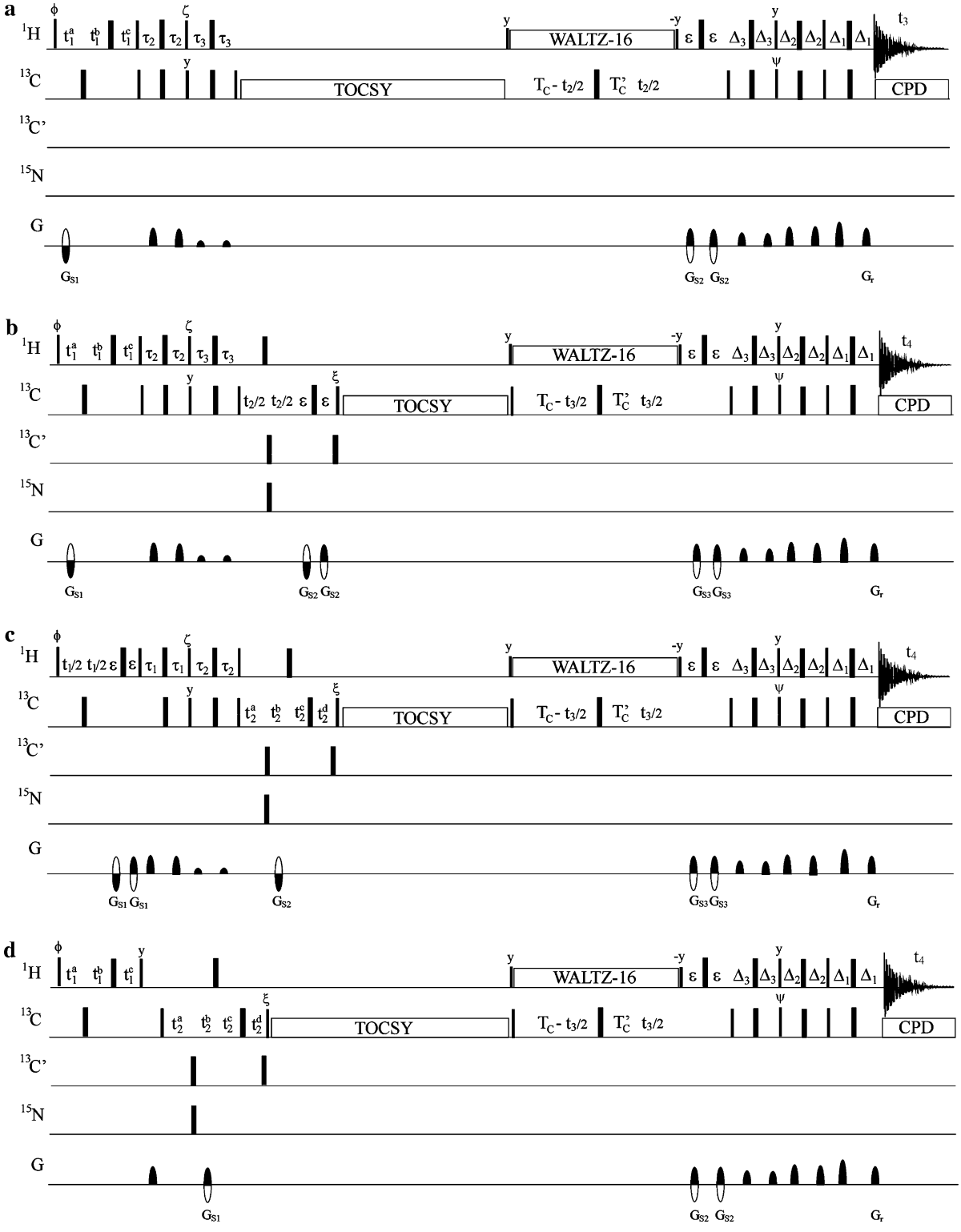
a
b
c
d
WALTZ-16
TOCSY
CPD

Figure 1. HCCmHm-TOCSY experiments for the sequence-specific assignment of Ala, Ile, Leu, Thr and Val residues in $^{13}C/(^{15}N)$ labeled proteins. Narrow and wide bars correspond to 90° and 180° flip angles, respectively, applied with phase x unless otherwise stated. All 90° and 180° pulses for aliphatic carbons were applied with a strength of 20.8 kHz. The ^{1}H, ^{15}N, and $^{13}C'$ carrier positions are 2.9 (center of aliphatic proton region), 120 (center of ^{15}N spectral region), and 175 ppm (center of $^{13}C'$ spectral region). The $^{13}C'$ carrier is set initially to the middle of aliphatic ^{13}C region (39 ppm) and shifted to 20 ppm just after the TOCSY mixing sequence. A) 3D double sensitivity-enhanced, gradient selected GDE-H(C)CmHm-TOCSY experiment. Delay durations: $t_1^a = \tau_1 + t_1/2, t_1^b = (1-\kappa) * t_1/2, t_1^c = \tau_1 - \kappa * t_1/2, \tau_1 = 1/(4J_{HC}) \sim 1.7$ ms; $\tau_2 = 1.1$ ms; $\tau_3 = 0.9$ ms; $\Delta_1 = 1/(4J_{CmHm}) \sim 2.0$ ms; $\Delta_2 = 0.6$ ms; $\Delta_3 = 0.76$ ms; $T_C = 1/(2J_C\alpha_C\beta) \sim 14$ ms; $T'_C = T_C - 2\varepsilon$; ε = gradient + field recovery delay; $0 \leq \kappa \leqslant 2\tau_1/t_{1,max}$. Frequency discrimination in F_1 and F_2 is obtained using sensitivity-enhanced gradient selection (Kay et al., 1992; Schleucher et al., 1993). The echo and antiecho signals in F_1 and F_2 dimensions are collected separately by inverting the sign of the G_{S1} and G_{S2} gradient pulses together with the inversion of ζ, and ψ and ζ, respectively. Phase settings: ϕ = x; ψ = −y, y; ξ = y, −y, −y, y. Gradient strengths: G_{S1} = 1 k G/cm, G_{S2} = 18 k G/cm, G_r = 10 k G/cm. Gradient duration: 0.4 ms. B) 4D triple sensitivity-enhanced, gradient selected GTE-HCCmHm-TOCSY with zxy-ICOS-CT element. Delay durations as in A). Quadrature detection in F_1, F_2, and F_3 is obtained using sensitivity-enhanced gradient selection. Eight datasets are collected separately by inverting the sign of the G_{S1}, G_{S2} and G_{S3} gradient pulses together with the inversion of ζ, ξ and ζ, and ψ and ξ, respectively. Phase settings: ϕ = x; ψ = −y, y; ξ = −x, x, x, −x. ζ = 2(y), 4(−y), 2(y). Gradient strengths: G_{S1} = 2.7 k G/cm, G_{S2} = 2.6 k G/cm, G_{S3} = 18 k G/cm, G_r = 13 k G/cm. C) 4D triple sensitivity-enhanced, gradient selected GTE-HCCmHm-TOCSY with yxz-ICOS-CT element. Delay durations: $\tau_1 = 1/(4J_{HC}) \sim 1.7$ ms; $\tau_2 = 0.9$ ms; $\tau_3 = 1.1$ ms; $t_2^a = t_1/2; t_2^b = \tau_3$, $t_2^c = (1-\lambda) * t_2/2, t_2^d = \tau_3 - \lambda * t_2/2; 0 \leq \lambda \leq 2\tau_3/t_{2,max}$. Gradient strengths: G_{S1} = 1.3 k G/cm, G_{S2} = −5.1 k G/cm, G_{S3} = 18 k G/cm, G_r = 13 k G/cm. Quadrature detection with the phase settings as in B). D) 4D double sensitivity-enhanced, gradient selected GDE-HCCmHm-TOCSY experiment. Delay durations $t_1^a = \tau_1 + t_1/2, t_1^b = (1-\kappa) * t_1/2, t_1^c = \tau_1 - \kappa * t_1/2, \tau_1 = 1/(4J_{HC}) \sim 1.7$ ms; $t_2^a = t_1/2, t_2^b = \tau_3, t_2^c = (1-\lambda) * t_2/2, t_2^d = \tau_3 - \lambda * t_2/2$; $0 \leq \lambda \leq 2\tau_3/t_{2,max}, \tau_3 = 1/(4J_{CH}) \sim 1.1$ ms. Gradient strengths: G_{S1} = 3.6 k G/cm, G_{S2} = 18 k G/cm, G_r = 10 k G/cm. Phase settings: $\phi = 45°$; ψ = −y, y; ξ = −x, x, x, −x. Frequency discrimination in F_1 is obtained using States-TPPI protocol (Marion et al., 1989) applied to ϕ, whereas quadrature detection in F_2 and F_3 is accomplished by sensitivity-enhanced gradient selection. The echo and anti-echo signals are collected separately by inverting the sign of G_{S1} and G_{S2} gradient pulses together with the inversion of ξ, and ψ and ξ, respectively. The DIPSI-3 spin-lock (9 kHz) was employed for ^{13}C-^{13}C transfer. The WALTZ-16 sequence (Shaka et al., 1983) was used to decouple ^{1}H spins during $2T_C$. The adiabatic WURST field (Kupće and Wagner, 1995) was used to decouple ^{13}C during acquisition.

of carbons before the TOCSY mixing sequence is omitted in the three-dimensional version of the experiment (see Figure 1a). The subsequent TOCSY mixing sequence can be used for transferring both orthogonal x and z components (or x and y components in the three-dimensional scheme) of magnetization to methyl $^{13}C_m$ spins i.e. establishing a $^{13}C^+ \rightarrow {}^{13}C_m^+$ transfer. Hence, the theoretical sensitivity improvement by a factor sqrt(2), irrespective of the spin system, is obtained with respect to the conventional hypercomplex frequency discrimination in which the phase-sensitive signal is obtained by combining two amplitude modulated signals in t_2 (Cavanagh and Rance, 1990; Sattler et al., 1995b; Kövér et al., 1998). The 90° pulse on ^{13}C following the TOCSY sequence converts the desired magnetization into $^{13}C_m^+$ coherence which evolves during the t_3 (t_2 in the three-dimensional experiment) evolution period. Methyl carbon chemical shift evolution takes place during a constant-time period of 27 ms, which provides an outstanding resolution in the methyl carbon dimension. The use of a constant-time approach can readily be justified as the transverse relaxation times of methyl carbons are very long even in large non-deuterated proteins, thanks to the fast spin rotation of methyl groups. Proton spin flips during the long $2T_C$ period induce an effective transverse relaxation mechanism for methyl carbon. This can be inhibited by applying sensitivity enhancing proton decoupling during most of the $2T_C$ period (Uhrín et al., 2000). An additional pair of dephasing gradients (G_S3) is employed during the t_3 period in order to achieve coherence selection and quadrature detection in t_3. A 180°(^{1}H) pulse is applied between the two gradient pulses to prevent J coupling evolution during the gradient echo (Permi et al., 2004). In the final step, $^{13}C_m^+$ coherence is transferred to observable $^{1}H_m^-$ coherence prior to the acquisition period by employing the yxz-ICOS-CT sequence. In this way, both orthogonal magnetization components can be transferred from methyl carbon to methyl proton.

Prior to acquisition, the signal of interest is purely phase modulated in all three indirectly detected dimensions i.e. $\exp(\pm i\omega_H t_1) \exp(\pm i\omega_C t_2) \exp(\pm i\omega_{Cm} t_3)$ in four-dimensional or $\exp(\pm i\omega_H t_1) \exp(\pm i\omega_{Cm} t_2)$ in three-dimensional experiments. Sensitivity-enhanced gradient selection has been applied to all three indirectly detected dimensions, which enables recording of a four-dimensional

spectrum using only one transient. For the triple sensitivity-enhanced four-dimensional pulse sequence, eight separate experiments are required with echo (E) - antiecho (A) selection in all three indirect dimensions:

$$\mathrm{A/A/A}: \quad H_m^- \exp(i\omega_H t_1) \exp(i\omega_C t_2) \exp(i\omega_{Cm} t_3) \exp(i\omega_{Hm} t_4) \tag{1}$$

$$\mathrm{E/E/A}: \quad H_m^- \exp(i\omega_H t_1) \exp(-i\omega_C t_2) \exp(i\omega_{Cm} t_3) \exp(i\omega_{Hm} t_4) \tag{2}$$

$$\mathrm{E/A/A}: \quad H_m^- \exp(-i\omega_H t_1) \exp(i\omega_C t_2) \exp(i\omega_{Cm} t_3) \exp(i\omega_{Hm} t_4) \tag{3}$$

$$\mathrm{A/E/E}: \quad H_m^- \exp(i\omega_H t_1) \exp(i\omega_C t_2) \exp(-i\omega_{Cm} t_3) \exp(i\omega_{Hm} t_4) \tag{4}$$

$$\mathrm{A/A/E}: \quad H_m^- \exp(-i\omega_H t_1) \exp(-i\omega_C t_2) \exp(-i\omega_{Cm} t_3) \exp(i\omega_{Hm} t_4) \tag{5}$$

$$\mathrm{E/A/E}: \quad H_m^- \exp(i\omega_H t_1) \exp(-i\omega_C t_2) \exp(-i\omega_{Cm} t_3) \exp(i\omega_{Hm} t_4) \tag{6}$$

$$\mathrm{A/E/A}: \quad H_m^- \exp(-i\omega_H t_1) \exp(-i\omega_C t_2) \exp(i\omega_{Cm} t_3) \exp(i\omega_{Hm} t_4) \tag{7}$$

$$\mathrm{E/E/E}: \quad H_m^- \exp(-i\omega_H t_1) \exp(i\omega_C t_2) \exp(-i\omega_{Cm} t_3) \exp(i\omega_{Hm} t_4) \tag{8}$$

Eight signals are produced with equal intensity resulting in a signal-to-noise ratio increased theoretically by a factor of sqrt(8) with respect to a standard four-dimensional pulse scheme. In practice, however, the S/N ratio will not be increased by the theoretical factor due to differing spin multiplicities, homonuclear $^1J_{CC}$ couplings, relaxation effects and larger number of RF pulses (*vide infra*). An appropriate Fourier transform i.e. by manipulating the data according to the sensitivity-enhanced procedure in all three indirectly detected dimensions yields correlations at $\omega_H(i)$, $\omega_C(i)$, $\omega_{Cm}(i)$, $\omega_{Hm}(i)$.

For the three-dimensional double sensitivity-enhanced experiment, four different data sets are collected:

$$\mathrm{A/A}: \quad H_m^- \exp(i\omega_H t_1) \exp(i\omega_{Cm} t_2) \exp(i\omega_{Hm} t_3) \tag{9}$$

$$\mathrm{E/A}: \quad H_m^- \exp(-i\omega_H t_1) \exp(i\omega_{Cm} t_2) \exp(i\omega_{Hm} t_3) \tag{10}$$

$$\mathrm{A/E}: \quad H_m^- \exp(-i\omega_H t_1) \exp(-i\omega_{Cm} t_2) \exp(i\omega_{Hm} t_3) \tag{11}$$

$$\mathrm{E/E}: \quad H_m^- \exp(i\omega_H t_1) \exp(-i\omega_{Cm} t_2) \exp(i\omega_{Hm} t_3) \tag{12}$$

The theoretical increase in the S/N ratio by a factor of 2 is obtained with respect to a non-sensitivity enhanced three-dimensional experiment. Fourier transform in the sensitivity-enhanced echo-antiecho manner yields cross peaks at $\omega_H(i)$, $\omega_{Cm}(i)$, $\omega_{Hm}(i)$.

Materials and methods

The proposed four- and three-dimensional pulse schemes were recorded on 0.8 mM uniformly ^{15}N, ^{13}C labeled coactosin having a molecular mass of 16 kDa (142 residues), dissolved in D_2O, 10 mM Bis-Tris buffer (pH 6.0), 50 mM NaCl, 1 mM DTT in a 260 µl Shigemi microcell at 25°C. Experiments in Figure 1a, 1b and 1d were carried out on a Varian Unity INOVA 600 NMR spectrometer, equipped with a $^{15}N/^{13}C/^1H$ triple-resonance coldprobe and an actively shielded z-axis gradient system. Experiment in Figure 1c was carried out on a Varian Unity INOVA 500 NMR spectrometer for testing purpose only. The spectrometer is equipped with a conventional $^{15}N/^{13}C/^1H$ triple-resonance probehead and an actively shielded z-axis gradient system. Acquisition parameters for the measured three-dimensional and four-dimensional spectra are given in

Table 1. Prior to zero-filling and Fourier transformation, four-dimensional data were extended by two-fold in each indirectly detected dimension using a forward-backward linear prediction algorithm implemented into the NMRPipe software package (Delaglio et al., 1995). Spectra were analyzed using NMRDraw included in the NMRPipe package. Isotropic DIPSI-3 TOCSY sequence (Shaka et al., 1988) with a 12.2 ms mixing time was utilized for ^{13}C–^{13}C transfer.

Results and discussion

It has been shown earlier that no uniform sensitivity improvement by a factor of sqrt(2) can be retrieved for IS, I_2S and I_3S spin moieties simultaneously, since coherence transfer cannot be optimized for different effective Hamiltonians during the heteronuclear coherence transfer using a single set of mixing times (Sattler et al., 1995b). The three COS-CT steps of the proposed three-dimensional GDE-H(C)CmHm-TOCSY and four-dimensional GTE-HCCmHm-TOCSY experiments (Figure 1a–b) are designed to get the best of the coherence transfer step in terms of sensitivity. In the first magnetization transfer step from proton to carbon, we are aiming for optimizing the sensitivity for HC and H_2C spin moieties. To this end, the zxy-ICOS-CT pulse element is employed with appropriate delay settings, i.e. $\tau_1 = 1/(4J_{HC})$, $\tau_2 = 1.1$ ms, and $\tau_3 = 0.9$ ms. According to the theory, a gain in sensitivity by a factor of 1.3 and 1.25 is obtained for HC and H_2C groups, respectively. The second magnetization transfer step involves a homonuclear isotropic mixing sequence, e.g. DIPSI-3 (Shaka et al., 1988), which can be used for obtaining a sensitivity improvement by a theoretical factor of sqrt(2), irrespective of the spin system, in comparison to a z-filtered TOCSY mixing sequence. The final transfer step is composed of an in-phase yxz-ICOS-CT heteronuclear mixing sequence to transfer methyl carbon coherence to methyl protons. Despite this transfer is less than optimal for I_3S moieties as determined by the unitary bound on spin dynamics for Hermitian matrices (Sørensen, 1990, 1991; Sattler et al., 1995b; Untidt et al., 1998), calculations suggest a sensitivity improvement by a factor of 1.22 (omitting the sensitivity loss due to relaxation and RF field inhomogeneity) with respect to refocused INEPT (Permi et al., 2004). Optimal sensitivity for CH_3 moieties during the final transfer step is attained by setting delays $2\Delta_1$, $2\Delta_2$, and $2\Delta_3$ to $0.5/J_{CmHm}$, $0.153/J_{CmHm}$ and $0.196/J_{CmHm}$, where J_{CmHm} is the heteronuclear one-bond coupling between methyl carbon and proton. Relaxation during the final yxz-ICOS-CT element does not pose a serious problem in methyl groups since the transverse relaxation rates for $^{13}C_m$ and $^{1}H_m$ spins are relatively low even in larger proteins. Indeed, we have shown earlier that the double sensitivity-enhanced DE-MQ-(H)CCmHm-TOCSY experiment improved the sensitivity of the conventional MQ-(H)CCmHm-TOCSY on average by a factor of 1.6 for a protein with a rotational correlation time of 14.5 ns (Permi et al., 2004).

To sum up the above concepts, the triple sensitivity-enhanced four-dimensional GTE-HCCm Hm-TOCSY experiment provides superior resolution in comparison to its three-dimensional, double sensitivity-enhanced counterparts, the DE-MQ-(H)CCmHm-TOCSY scheme (Permi et al., 2004) and the proposed three-dimensional GDE-H(C)CmHm-TOCSY experiment (Figure 1a). The sensitivity of the four-dimensional GTE-HCCmHm-TOCSY (Figure1b) experiment is comparable to that of the three-dimensional GDE-H(C)CmHm-TOCSY experiment (Figure1a) if the sensitivity loss due to ^{13}C transverse relaxation and $^{1}J_{CC}$ modulation during t_2 and the subsequent gradient defocusing delay 2ε is neglected. Thus, an inherent sensitivity loss by a factor of sqrt(2) due

Table 1. Acquisition parameters used for 3D and 4D HCCmHm-TOCSY experiments

Experiment	Number of complex points (t_1, t_2, t_3, t_4)	Acquisition times (t_1, t_2, t_3, t_4) [ms]	Number of transients	Experimental time [h]
Figure 1a	56, 60, 256	13.7, 26.1, 51.1	2	9
Figure 1b	26, 22, 40, 256	6.4, 2.3, 17.4, 51.1	1	52
Figure 1d	16, 16, 28, 256	3.9, 1.7, 12.2, 51.1	1	16

to the additional incremented dimension is counterbalanced by the sensitivity-enhanced gradient selection, which is followed by the homonuclear isotropic mixing sequence. However, use of the zxy-ICOS-CT mixing sequence between the t_1 and t_2 periods establishes also a COSY-like coherence transfer between neighboring ^{13}C spins during the delay $2\tau_2$ (Figure 1b). Using density operator presentation, this conversion can be described in the following way for a CH–CH_3 moiety found in Ala residues.

$$\begin{aligned}
&H_zC_y^1 \xrightarrow{2\tau_2(^1J_{CH}+^1J_{CC})} C_y^1C_z^2\sin(2\pi J_{CH}\tau_2)\sin(2\pi J_{CC}\tau_2) \xrightarrow{90^\circ_y(^1H,^{13}C)} \\
&C_y^1C_x^2\sin(2\pi J_{CH}\tau_2)\sin(2\pi J_{CC}\tau_2) \xrightarrow{2\tau_3(^1J_{CH}+^1J_{CC})} \\
&C_y^1C_x^2\sin(2\pi J_{CH}\tau_2)\sin(2\pi J_{CC}\tau_2)\cos(2\pi J_{CH}\tau_3)\cos^3(2\pi J_{CmHm}\tau_3) \xrightarrow{90^\circ_x(^{13}C)} \\
&C_z^1C_x^2\sin(2\pi J_{CH}\tau_2)\sin(2\pi J_{CC}\tau_2)\cos(2\pi J_{CH}\tau_3)\cos^3(2\pi J_{CmHm}\tau_3)
\end{aligned} \tag{13}$$

where C^1 and C^2 correspond to α-carbon and methyl carbon spins, respectively. The outcome of the COSY-like transfer is a cross peak observable at $\omega_H(i)$, $\omega_{C\pm1}(i)$, $\omega_{Cm}(i)$, $\omega_{Hm}(i)$, where $\omega_{C\pm1}$ refers to ^{13}C spins preceding and following the carbon spin to which the origin ^1H spin is directly attached. In other words, additional two-bond correlations between the origin ^1H spin and the neighboring ^{13}C spins can be observed. This is exemplified in Figure 2 for residues Ala92 and Ile82 in a 16 kDa protein coactosin. Typically the COSY peaks are relatively weak (< 5–15%) with respect to the main peaks but in some cases their intensity can be comparable to the weaker TOCSY peaks as can be seen when comparing Ile82 Cγ1-Hγ12 and $C\gamma1 - H\gamma13$ TOCSY and $C\gamma2 - H\beta$ COSY correlations (Figure 2, upper right panel). These COSY correlations can be used to advantage in assignment, e.g. distinguishing between leucine and isoleucine residues due to their differing spin system topology or in cases of overlap. It is noteworthy that the coherence transfer leading to the COSY cross peaks is effective also during the three-dimensional GDE-H(C)CmHm-TOCSY experiment. However, absence of the additional ^{13}C dimension prevents observation of these correlations in the three-dimensional spectrum.

Emergence of the COSY peaks can be suppressed by using alternative coherence transfer schemes. In pulse sequence of Figure 1c this is achieved by employing the yxz-ICOS-CT scheme to transfer magnetization from ^1H to ^{13}C i.e. the relevant terms after the t_1 period for the CH-CH_3 moiety evolve during the yxz-ICOS element as follows

$$\begin{aligned}
&H_y + H_x \xrightarrow{90^\circ_x(^1H)-2\tau_1(^1J_{CH})-90^\circ_y(^1H,^{13}C)} H_x + H_yC_x^1\sin(2\pi J_{CH}\tau_1) \xrightarrow{2\tau_2(^1J_{CH}+^1J_{CC})} \\
&H_yC_z^1\sin(2\pi J_{CH}\tau_2) + H_yC_x^1\sin(2\pi J_{CH}\tau_1)\cos(2\pi J_{CC}\tau_2) + H_yC_y^1C_z^2\sin(2\pi J_{CH}\tau_1)\sin(2\pi J_{CC}\tau_2) \\
&\xrightarrow{90^\circ_x(^1H,^{13}C)} H_zC_y^1\sin(2\pi J_{CH}\tau_2) + H_zC_x^1\sin(2\pi J_{CH}\tau_1)\cos(2\pi J_{CC}\tau_2) \\
&+ H_zC_z^1C_x^2\sin(2\pi J_{CH}\tau_1)\sin(2\pi J_{CC}\tau_2)
\end{aligned} \tag{14}$$

As the antiphase $^2J_{CH}$ coupling will not be refocused during the ensuing semi-constant time delay $2\tau_3 + t_2$, the last term will not be converted to observable magnetization, and hence no COSY peaks are observed in the spectrum.

In this case, the first dephasing gradient (G_{S1}) cannot be incorporated into the first $^1J_{CH}$ dephasing delay i.e. an additional spin-echo period is required after t_1. Unlike the scheme in Figure 1b, the second dephasing gradient (G_{S2}) can be placed within the refocusing delay $2\tau_3$ and a semi constant-time evolution period can be utilized in

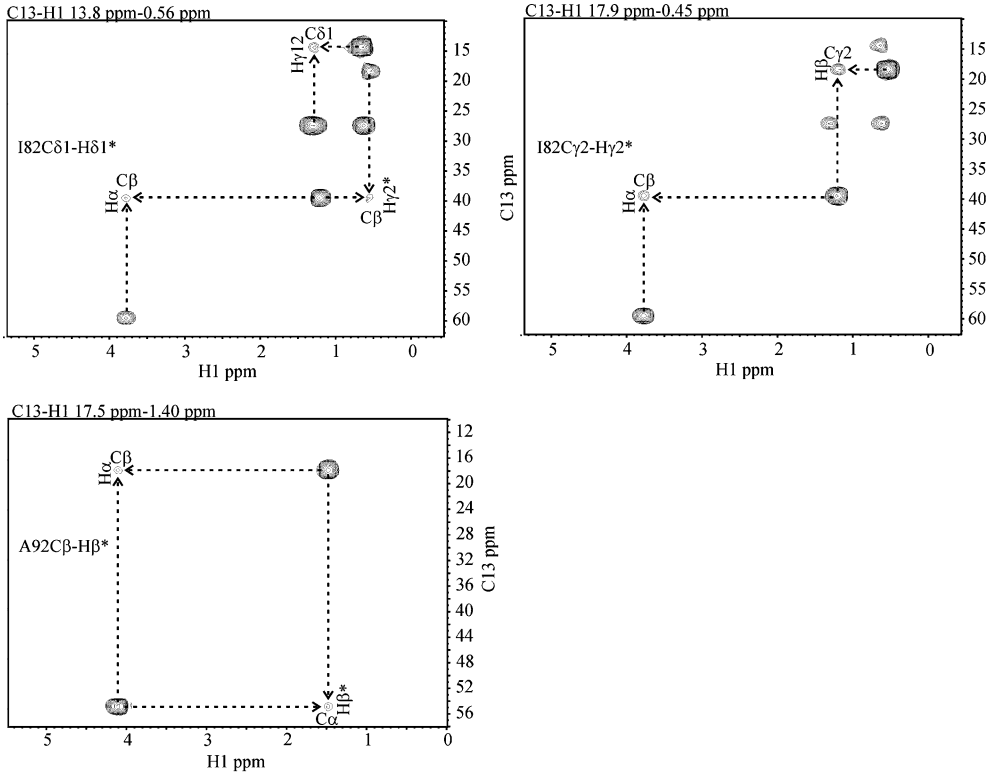

Figure 2. Representative $F_1(^1H)$–$F_2(^{13}C)$ planes of a four-dimensional HCCmHm-TOCSY spectrum acquired with the pulse sequence shown in Figure 1b. COSY peaks appear between ^1H and ^{13}C two bonds apart, due to evolution of homonuclear ^{13}C–^{13}C J coupling during the zxy-ICOS coherence transfer. In these examples the maximum COSY peak intensity (HαCβ) is 1/4 of that of the main cross peak (HαCα) for Ile82 (upper right panel). The spectrum was acquired from a 0.8 mM sample of the 16 kDa mouse protein coactosin in 52 h.

the ^{13}C (F_2) dimension. As a result, apparent transverse relaxation of ^{13}C spin as well as homonuclear ^{13}C–^{13}C coupling modulation are scaled down by a factor $\lambda = (t_{2,\max} - 2\tau_3)/t_{2,\max}$. The performance of the yxz-ICOS transfer is worse than the efficiency of the zxy-ICOS-CT element. In fact, the transfer efficiency with respect to the conventional INEPT transfer is improved by a factor of 1.2 for CH moieties, while the attainable sensitivity is 98% and 83% of the INEPT transfer for H_2C and H_3C moieties, respectively.

In the pulse sequence in Figure 1d, phase-sensitive quadrature detection in the ^1H dimension is obtained using a traditional States-TPPI detection (Marion et al., 1989). Thus, unlike its triple gradient selected counterparts in Figure 1b and 1c, the signal of interest in GDE-HCCmHm-TOCSY (Figure 1d) is $\cos(\omega_H t_1)$ or $\sin(\omega_H t_1)$ modulated in the F_1 dimension. The $^1H \rightarrow {}^{13}C$ transfer is accomplished by using a conventional INEPT transfer which purges COSY-like cross peaks by elimination of homonuclear coherence transfer prior to the t_2 evolution period i.e. only the $H_zC^1{}_y$ term will be modulated by the ^{13}C chemical shift during t_2.

In order to minimize the effect of ^1H and ^{13}C spin relaxation and ^{13}C-^{13}C J modulation, both t_1 and t_2 evolution periods are implemented in semi constant-time manner which also enables incorporation of the first dephasing gradient (G_{S1}) within the delay $2\tau_3$. The pulse scheme in Figure 1d is $2\varepsilon + 2\tau_2$ shorter than the pulse sequences utilizing the ICOS-CT elements and for this reason sensitivity loss occurring in large proteins arising from rapid relaxation of aliphatic, non-methyl carbons is minimized. Although no gradient is used for coherence selection in the F_1 dimension, the experiment can still be recorded using only one transient per FID as no isotope filtration is required in the first ^1H dimension. This keeps the experimental time short for a four-dimensional experiment. Interestingly, the sensitivity of the

four-dimensional GDE-HCCmHm-TOCSY is superior to the standard three-dimensional $H(C)CH_3$ and $(H)CCH_3$ TOCSY experiments (Uhrín et al. 2000) by a theoretical factor of 1.22 albeit an additional indirectly detected dimension is incremented. This can be understood by realizing that, to first approximation, the homonuclear ^{13}C-^{13}C TOCSY transfer between t_2 and t_3 evolution periods does not introduce any sensitivity loss. Table 2 summarizes the analytical transfer functions for different coherence transfer elements used in the proposed experiments for the $^1H \rightarrow {}^{13}C$ transfer.

We compared the attainable sensitivity of the three-dimensional GDE-H(C)CmHm-TOCSY experiment with that of the conventional $H(C)CH_3$-TOCSY scheme (Uhrín et al., 2000; Zheng et al., 2004). Figure 3 shows representative strip plots of Ile49, Val101, and Leu120 residues recorded with the pulse sequence in Figure 1a and with the $H(C)CH_3$-TOCSY scheme. The signal-to-noise ratio is increased on average by a factor of 1.4 with respect to the standard $H(C)CH_3$-TOCSY experiment (Uhrín et al., 2000; Zheng et al., 2004).

To demonstrate the feasibility and superior resolution of the four-dimensional HCCm-Cm-TOCSY experiments for the assignment of methyl-containing residues, we applied the pulse sequences to the uniformly $^{15}N/^{13}C$ labeled actin binding mouse coactosin, containing 142 residues (Hellman et al., 2004). Figure 4 illustrates portions of the three-dimensional GDE-H(C)CmHm-TOCSY and the four-dimensional GDE-HCCmHm-TOCSY spectra, recorded using the pulse sequences shown in Figure 1a and d, respectively. The $F_1(^1H)$ - $F_2(^{13}C)$ portions of the four-dimensional spectrum are taken at the frequencies of the methyl carbons (F_3) and protons (F_4), whereas the $F_1(^1H)$–$F_3(^1H)$ planes of the three-dimensional spectrum are taken at the chemical shift of the methyl carbon (F_2) of the corresponding residue. There are several forthcomings in the four-dimensional spectrum with respect to the three-dimensional editing. Each F_1-F_2 plane of the four-dimensional spectrum displays both proton and carbon chemical shifts within the spin system. Therefore, the four-dimensional approach provides direct ^1H–^{13}C connectivities for adjacent spins, that is, the ambiguity present in the assignment of aliphatic

Table 2. Analytical transfer functions for zxy-ICOS-CT (Figure 1a-b), yxz-ICOS-CT (Figure 1c) and INEPT (Figure 1d) elements in HC–C, C–H_2C–C and H_3C–C spin moieties

	HC–C	C–H_2C–C	H_3C–C
Figure 1a and b	$\sin(2\pi J_{CH}\tau_1)\cos(2\pi J_{CC}\tau_2)[\sin(2\pi J_{CH}\tau_3)\cos(2\pi J_{CH}\tau_3) + \sin(2\pi J_{CH}\tau_2)]$	$\sin(2\pi J_{CH}\tau_1)\cos(2\pi J_{CH}\tau_2)\cos^2(2\pi J_{CC}\tau_2)[\sin(2\pi J_{CH}\tau_3)\cos(2\pi J_{CH}\tau_3)\cos^2(2\pi J_{CC}\tau_3) + \sin(2\pi J_{CH}\tau_2)]$	$\sin(2\pi J_{CH}\tau_1)\cos^2(2\pi J_{CH}\tau_2)\cos(2\pi J_{CC}\tau_2)[\sin(2\pi J_{CH}\tau_3)\cos^2(2\pi J_{CH}\tau_3)\cos(2\pi J_{CC}\tau_3) + \sin(2\pi J_{CH}\tau_2)]$
Figure 1c	$\sin(2\pi J_{CH}\tau_3)\cos(2\pi J_{CC}\tau_3)[\sin(2\pi J_{CH}\tau_1)\cos(2\pi J_{CC}\tau_2) + \sin(2\pi J_{CH}\tau_2)]$	$\sin(2\pi J_{CH}\tau_3)\cos(2\pi J_{CH}\tau_3)\cos^2(2\pi J_{CC}\tau_3)[\sin(2\pi J_{CH}\tau_1)\cos(2\pi J_{CH}\tau_2)\cos^2(2\pi J_{CC}\tau_2) + \sin(2\pi J_{CH}\tau_2)]$	$\sin(2\pi J_{CH}\tau_3)\cos^2(2\pi J_{CH}\tau_3)\cos(2\pi J_{CC}\tau_3)[\sin(2\pi J_{CH}\tau_1)\cos^2(2\pi J_{CH}\tau_2)\cos(2\pi J_{CC}\tau_2) + \sin(2\pi J_{CH}\tau_2)]$
Figure 1d	$\sin(2\pi J_{CH}\tau_1)\sin(2\pi J_{CH}\tau_3)\cos(2\pi J_{CC}\tau_3)$	$\sin(2\pi J_{CH}\tau_1)\sin(2\pi J_{CH}\tau_3)\cos^2(2\pi J_{CH}\tau_3)(2\pi J_{CC}\tau_3)\cos(2\pi J_{CH}\tau_3)$	$\sin(2\pi J_{CH}\tau_1)\cos^2(2\pi J_{CH}\tau_3)\cos(2\pi J_{CC}\tau_3)\sin(2\pi J_{CH}\tau_3)$

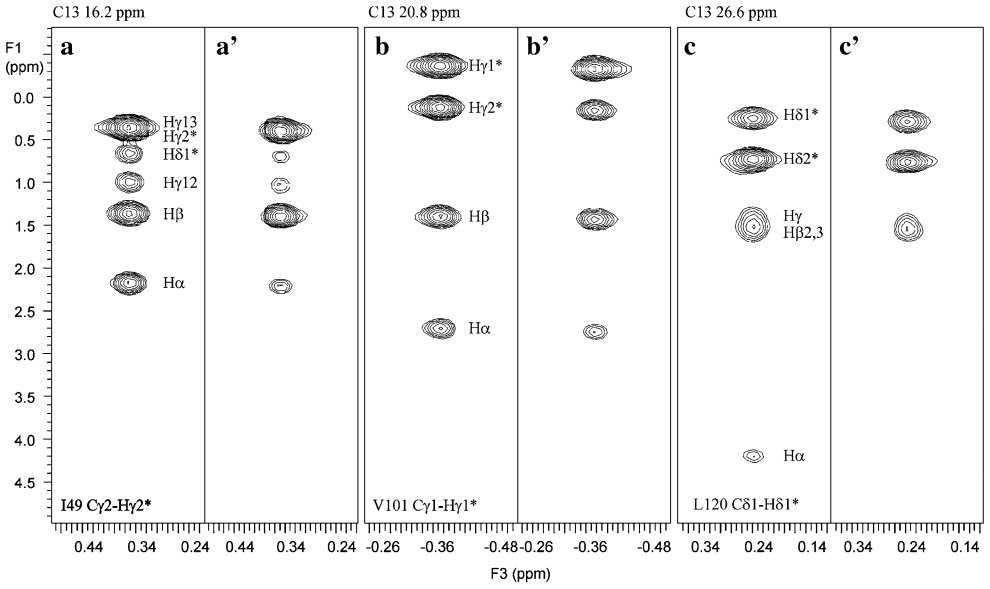

Figure 3. Comparison of three-dimensional H(C)CmHm-TOCSY spectra of mouse coactosin. Three representative pairs of two dimensional $F_1(^1H)$–$F_3(^1H)$ planes are shown with the GDE-H(C)CmHm-TOCSY experiment (Figure 1a) on the left (a–c) and the conventional H(C)CH_3-TOCSY experiment (Uhrín et al., 2000, Zheng et al., 2004) on the right (a′-c′). The higher signal-to-noise ratio in the GDE-H(C)CmHm-TOCSY spectrum is obvious.

^{1}H resonances is greatly reduced by the additional information on the chemical shift of their directly attached carbons. For example, in the case of Leu100 CγHγ and CβHβ chemical shifts can readily be assigned unambiguously (Figure 4a–b). Also, overlap is significantly reduced, as exemplified by Ile82 Hβ, Hγ and Hδ chemical shifts in Figure 4c–d or for Val37 in Figure 4e–f. In comparison to the GTE-HCCmHm-TOCSY spectrum shown in Figure 2, it can be realized that all COSY-like correlations within the spin system are absent. The spectra shown in Figures 2–4 were measured on a 600 MHz spectrometer equipped with a cryogenically cooled probehead. The four-dimensional GDE-HCCmHm-TOCSY experiment was executed using a single transient per FID, yielding a total measurement time of only 16 hours. This turned out to be adequate for assigning all the 77 methyl groups found in coactosin i.e. 15 Ala, 7 Leu, 8 Ile, 11 Val, and 10 Thr residues. In comparison, the three-dimensional GDE-H(C)CmHm-TOCSY and H(C)CH_3-TOCSY spectra were recorded using two scans per FID with a measurement time of 9 hours per experiment. The pulse scheme in Figure 1c was experimentally verified on a 500 MHz spectrometer equipped with a conventional probehead. Despite the inherently lower sensitivity and resolution attainable, the assignment could be performed equally efficiently with the same results (data not shown). By taking the 3.25 times longer experimental time into account, the four-dimensional GTE-HCCmHm-TOCSY (Figure 1b) in our hands provided a 1.2 – 1.4 times higher sensitivity in comparison to the GDE-HCCmHm-TOCSY (Figure1d). It can be anticipated that this sensitivity enhancement, obtained using the ICOS ^{1}H-^{13}C coherence transfer between t_1 and t_2 evolution periods, will be lost on larger proteins (> 20–25 kDa) where transverse relaxation time of aliphatic methine/methylene protons and carbons becomes prohibitively fast. Consequently, the attainable sensitivity of the GDE-HCCmHm-TOCSY experiment (Figure 1d) that employs only homonuclear ^{13}C–^{13}C and heteronuclear methyl ^{13}C–^{1}H ICOS transfer becomes superior to the GTE-HCCmHm-TOCSY experiments (Figure 1b–c) on large proteins. As we have shown earlier, the use of homonuclear ^{13}C–^{13}C and heteronuclear methyl ^{13}C–^{1}H ICOS transfer is advantageous for proteins with correlation times up to at least 15 ns (Permi et al., 2004). In addition,

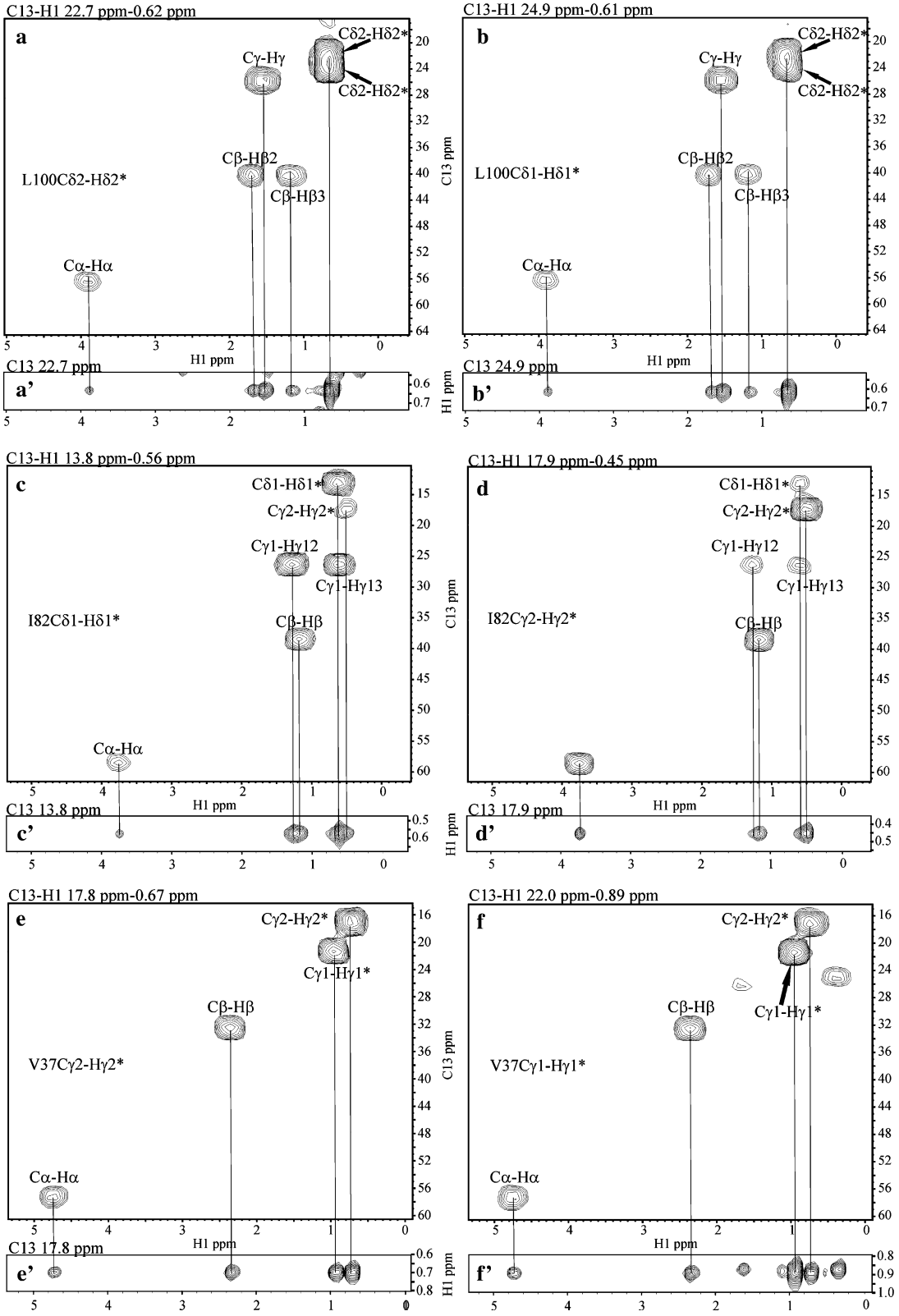
C13-H1 22.7 ppm-0.62 ppm
a
Cδ2-Hδ2*
Cγ-Hγ
Cδ2-Hδ2*
Cβ-Hβ2
L100Cδ2-Hδ2*
Cβ-Hβ3
Cα-Hα
H1 ppm
C13 22.7 ppm
a'
C13-H1 24.9 ppm-0.61 ppm
b
Cδ2-Hδ2*
Cγ-Hγ
Cδ2-Hδ2*
Cβ-Hβ2
L100Cδ1-Hδ1*
Cβ-Hβ3
Cα-Hα
C13 ppm
H1 ppm
C13 24.9 ppm
b'
C13-H1 13.8 ppm-0.56 ppm
c
Cδ1-Hδ1*
Cγ2-Hγ2*
Cγ1-Hγ12
Cγ1-Hγ13
I82Cδ1-Hδ1*
Cβ-Hβ
Cα-Hα
H1 ppm
C13 13.8 ppm
c'
C13-H1 17.9 ppm-0.45 ppm
d
Cδ1-Hδ1*
Cγ2-Hγ2*
Cγ1-Hγ12
Cγ1-Hγ13
I82Cγ2-Hγ2*
Cβ-Hβ
C13 ppm
H1 ppm
C13 17.9 ppm
d'
C13-H1 17.8 ppm-0.67 ppm
e
Cγ2-Hγ2*
Cγ1-Hγ1*
Cβ-Hβ
V37Cγ2-Hγ2*
Cα-Hα
H1 ppm
C13 17.8 ppm
e'
C13-H1 22.0 ppm-0.89 ppm
f
Cγ2-Hγ2*
Cγ1-Hγ1*
Cβ-Hβ
V37Cγ1-Hγ1*
Cα-Hα
C13 ppm
H1 ppm
f'

Figure 4. Comparison of three-dimensional GDE-H(C)CmHm-TOCSY (Figure 1a) and four-dimensional GDE-HCCmHm-TOCSY (Figure 1d) spectra of mouse coactosin. $F_1(^1H)$–$F_3(^1H)$ slices of the three-dimensional GDE-H(C)CmHm-TOCSY spectrum (a′– f′, lower panels) are aligned with $F_1(^1H)$–$F_2(^{13}C)$ planes of the four-dimensional GDE-HCCmHm-TOCSY spectrum (a–f, upper panels). Acquisition time was 13.7 ms (3.9 ms extended to 7.8 ms by linear prediction) in the F_1 dimension of the three-dimensional (four-dimensional) spectrum. The acquisition time in the F_2 dimension of the four-dimensional spectrum was 1.7 ms, which was extended to 3.4 ms by linear prediction prior to Fourier transform. The superiority of the four-dimensional approach is apparent in the case of Ile82 (c–d), where all protons can be linked to their directly bound carbons. In contrast, the three-dimensional spectrum exhibits heavily overlapping resonances (c′-d′). The spectra were acquired in 9 (3D) and 16 (4D) h.

the GDE-HCCmHm-TOCSY (Figure 1d) scheme does not produce COSY like correlations, which can be critical in large proteins exhibiting an increasing number of overlapping cross peaks.

Conclusions

Assignment of methyl-containing residues in proteins is vital as these provide the vast majority of long-range NOE connectivities for protein structure calculations. We have introduced a set of HCCmHm-TOCSY experiments, which can be employed for unambiguous assignment of methyl-containing residues. The proposed three-dimensional GDE-H(C)CmHm-TOCSY scheme is complementary to the earlier DE-MQ-(H)CCmHm-TOCSY experiment (Permi et al., 2004) as it supplements aliphatic ^{13}C, methyl $^1H/^{13}C$ connectivities with the corresponding aliphatic ^1H, methyl $^1H/^{13}C$ correlations. However, these experiments do not provide direct methine/methylene ^1H, ^{13}C connectivities. As a remedy, we have introduced a sensitive four-dimensional approach in this paper. These novel pulse schemes benefit from gradient selection and sensitivity enhancement in two or three indirectly detected dimensions, enabling the use of only a single transient per FID. This makes recording of high-resolution four-dimensional spectra viable using a reasonable amount of spectrometer time. We have shown that a complete sidechain assignment of methyl-containing residues can be accomplished for a 16 kDa protein using a four-dimensional spectrum recorded in 16 hours at 600 MHz using one transient. With these experiments the size limit of proteins amenable to sidechain methyl assignment is extended, without any costly selective labeling procedure. In addition, automated sidechain assignment programs greatly benefit from increased resolution in the four-dimensional spectrum.

Acknowledgments

This work was financially supported by the grant 106852 (P. P.) from the Academy of Finland.

References

Bax, A., Clore, M., Driscoll, P.C., Gronenborn, A.M., Ikura, M. and Kay, L.E. (1990a) *J. Magn. Reson.* **87**, 620–627.
Bax, A., Clore, M. and Gronenborn, A.M. (1990b) *J. Magn. Reson.* **88**, 425–431.
Cavanagh, J. and Rance, M. (1990) *J. Magn. Reson.* **88**, 72–85.
Clowes, R.T., Boucher, W., Hardman, C.H., Domaille, P.J. and Laue, E.D. (1993) *J. Biomol. NMR* **3**, 349–354.
Delaglio, F., Grzesiek, S., Vuister, G.W., Zhu, G., Pfeifer, J. and Bax, A. (1995) *J. Biomol. NMR* **6**, 277–293.
Fesik, S.W., Eaton, H.L., Olejniczak, E.T. and Zuiderweg, E.R.P. (1990) *J. Am. Chem. Soc.* **112**, 886–888.
Gardner, K.H., Konrat, R., Rosen, M.K. and Kay, L.E. (1996) *J. Biomol. NMR* **8**, 351–356.
Gardner, K.H., Rosen, M.K. and Kay, L.E. (1997a) *Biochemistry* **36**, 1389–1401.
Gardner, K.H., Zhang, X., Gehring, K. and Kay, L.E. (1997b) *J. Am. Chem. Soc.* **120**, 11738–11758.
Goto, N.K., Gardner, K.H., Mueller, G.A., Willis, R.C. and Kay, L.E. (1999) *J. Biomol. NMR* **13**, 369–374.
Grzesiek, S., Anglister, J. and Bax, A. (1993) *J. Magn. Reson.* **101**, 114–119.
Grzesiek, S. and Bax, A. (1993) *J. Biomol. NMR* **3**, 185–204.
Hajduk, P.J., Augeri, D.J., Mack, J., Mendoza, R., Yang, J., Betz, S.F. and Fesik, S.W. (2000) *J. Am. Chem. Soc.* **122**, 7898–7904.
Hellman, M., Paavilainen, V.O., Naumanen, P., Annila, A., Lappalainen, P. and Permi, P. (2004) *FEBS Lett.* **576**, 91–96.
Hilty, C., Fernandez, C., Wider, G. and Wüthrich, K. (2002) *J. Biomol. NMR* **23**, 289–301.
Kay, L.E., Ikura, M., Tschudin, R. and Bax, A. (1990a) *J. Magn. Reson.* **89**, 496–514.
Kay, L.E., Ikura, M. and Bax, A. (1990b) *J. Am. Chem. Soc.* **112**, 888–889.
Kay, L.E., Keifer, P. and Saarinen, T. (1992) *J. Am. Chem. Soc.* **114**, 10663–10665.
Kövér, K., Uhrín, D. and Hruby, V. (1998) *J. Magn. Reson.* **130**, 162–168.
Kupće, E. and Wagner, G. (1995) *J. Magn. Reson.* **109A**, 329–333.
Liu, Y. and Wagner, G. (1999) *J. Biomol. NMR* **15**, 227–239.
Logan, T.M., Olejniczak, E.T., Xu, R.X. and Fesik, S.W. (1993) *J. Biomol. NMR* **3**, 225–231.

Lyons, B.A. and Montelione, G.T. (1993) *J. Magn. Reson.* **101**, 206–209.
Marion, D., Ikura, M., Tschudin, R. and Bax, A. (1989) *J. Magn. Reson.* **85**, 393–399.
Montelione, G.T., Lyons, B.A., Emerson, S.D. and Tashiro, M. (1992) *J. Am. Chem. Soc.* **114**, 10974–10975.
Mueller, G.A., Choy, W.Y., Yang, D., Forman-Kay, J.D., Venters, R.A. and Kay, L.E. (2000) *J. Mol. Biol.* **300**, 197–212.
Permi, P. and Annila, A. (2004) *Prog. Nucl. Magn. Reson. Spectr.* **44**, 97–137.
Permi, P., Tossavainen, H. and Hellman, M. (2004) *J. Biomol. NMR* **30**, 275–282.
Pervushin, K., Riek, R., Senn, H., Wider, G. and Wüthrich, K. (1997) *Proc. Natl. Acad. Sci. USA* **94**, 12366–12371.
Sattler, M., Schwedinger, M.G., Schleucher, J. and Griesinger, C. (1995a) *J. Biomol. NMR* **5**, 11–22.
Sattler, M., Schmidt, P., Schleucher, J., Schedletzky, O., Glaser, S.J. and Griesinger, C. (1995b) *J. Magn. Reson.* **108B**, 235–242.
Schleucher, J., Sattler, M. and Griesinger, C. (1993) *Angew. Chem. Int. Ed. Engl.* **32**, 1489–1491.
Shaka, A.J., Keeler, J., Frenkiel, T. and Freeman, R. (1983) *J. Magn. Reson.* **52**, 335–338.
Shaka, A.J., Lee, C.J. and Pines, A. (1988) *J. Magn. Reson.* **77**, 274–293.
Sørensen, O.W. (1990) *J. Magn. Reson.* **86**, 435–440.
Sørensen, O.W. (1991) *J. Magn. Reson.* **93**, 648–652.
Tugarinov, V. and Kay, L.E. (2003a) *J. Am. Chem. Soc.* **125**, 5701–5706.
Tugarinov, V. and Kay, L.E. (2003b) *J. Am. Chem. Soc.* **125**, 13868–13878.
Tugarinov, V., Sprangers, R. and Kay, L.E. (2004) *J. Am. Chem. Soc.* **126**, 4921–4925.
Uhrín, D., Uhrínová, S., Leadbeater, C., Nairn, J., Price, N. and Barlow, P. (2000) *J. Magn. Reson.* **142**, 288–293.
Untidt, T., Schulte-Herbrüggen, T., Luy, B., Glaser, S.J., Griesinger, C., Sørensen, O.W. and Nielsen, N.C. (1998) *Mol. Phys.* **95**, 787–796.
Yang, D., Zheng, Y., Liu, D. and Wyss, D.F. (2004) *J. Am. Chem. Soc.* **126**, 3710–3711.
Zheng, Y., Giovannelli, J.L., Ho, N.T., Ho, C. and Yang, D. (2004) *J. Biomol. NMR* **30**, 423–429.